Journal of Alloys and Compounds 509 (2011) 8215–8222

Contents lists available at ScienceDirect

Journal of Alloys and Compounds

journal homepage: www.elsevier.com/locate/jallcom

Effect of selective substitution of Co for Ni or Mn on the superstructure and microstructural properties of $Ni_{50}Mn_{29}Ga_{21}$

A. Satish Kumar, M. Ramudu, V. Seshubai*

School of Physics, University of Hyderabad, Hyderabad 500046, India

ARTICLE INFO

Article history:
Received 24 February 2011
Received in revised form 13 May 2011
Accepted 16 May 2011
Available online 23 May 2011

Keywords:
Ferromagnetic shape memory alloys
Calorimetry
Crystal structure
Microstructure
Ni–Mn–Ga–Co

ABSTRACT

Results from a systematic study of the effect of cobalt, selectively substituted for Ni and Mn, in the modulated orthorhombic (7 M) $Ni_{50}Mn_{29}Ga_{21}$ alloy are contrasted. Substitution of Co for Mn resulted in the stabilization of a non-modulated tetragonal (NM) phase at higher Co content. At lower Co contents, a mixture of 7 M and NM phases were found to co-exist. Increasing in Co content caused suppression of long-range twin deformation leading to sporadic islands within which twin variants were confined. These effects are attributed to the considerable stresses generated by an atomic volume change of 9.5% caused locally when Co is substituted for Mn. On the other hand, substitution of Co for Ni, which causes only 1.7% atomic volume change locally, was observed not to alter either the superstructural ordering or the long-range twin deformation. Our results show that the microstructures resultant on Co doping have a strong correlation to the structural ordering, which in turn depends on whether Co is substituted for Mn or for Ni, and also on the concentration of Co.

© 2011 Elsevier B.V. All rights reserved.

1. Introduction

Among Heusler alloys, the alloys of Ni–Mn–Ga system have been under active research owing to their multifunctional properties like large ferromagnetic and thermal shape memory effects [1–3], magneto-caloric effect [4] and magneto-resistance [5]. Alloying with another element influences both the crystal and electronic structures of the parent compound and affects the stability of austenitic and martensitic states; it can thus influence the physical properties drastically [6–10]. Magnetic field induced transformations from martensitic to austenitic states have been reported in $Ni_{50-x}Mn_{30}Ga_{20}Co_x$ ($x = 5, 7, 9$ and 13) [11]. A direct to inverse magnetic entropy change has been reported in $Ni_{50-x}Mn_yGa_{50-y}Co_x$ ($5 < x < 9$ and $30 < y < 32$), generated by appropriate tuning of composition leading to the existence of a paramagnetic gap [12]. These interesting phenomena stem from a strong dependence of structural and magnetic properties of these materials on composition, as well as on atomic order [13]. However, there has not been much understanding on the effect of Co substitution on the crystal structure, superstructural ordering and the associated microstructural properties of the alloys of Ni–Mn–Ga system, from a systematic study.

The off-stoichiometric Ni–Mn–Ga alloys crystallize in various structures depending on composition and thermo-mechanical treatments. In the austenitic phase, Ni_2MnGa compound has $L2_1$ atomic order, cubic with $Fm\bar{3}m$ space group [14]. The crystal structure of the martensitic phases in the above system has been reported to be tetragonal or monoclinic with five layered modulation (5 M) [15], orthorhombic or monoclinic with seven layered modulation (7 M) [16,17] or non-modulated tetragonal (NM) [14,18,19]. Among the martensitic phases, large magnetic-field-induced strain (MFIS) of 6% and 10% respectively has been reported in the 5 M and 7 M structures at considerably low stresses [1]. The stress levels required to cause considerable strain are very high in NM structures [20]. Gaitzsch et al. have shown that it is possible to stabilize either the 7 M or the NM structure for the same composition ($Ni_{50}Mn_{30}Ga_{20}$) by appropriate thermo-mechanical treatment [19]. In addition to having large magneto-crystalline anisotropy, it is essential for a material to exhibit favorable structural ordering and microstructural (twin deformation) properties for rendering it suitable for shape memory applications [1,21]. Considerable strain deformation and large recovery ratio have been observed in polycrystalline $Ni_{53.5}Mn_{26.0}Ga_{20.5}$ alloy that crystallizes in 7 M monoclinic structure with magneto-structural transformation, owing to low residual stresses and multimode twinning [22]. Recent Electron Backscatter Diffraction (EBSD) studies report further insight into the orientation relations between twin variants in $Ni_{50}Mn_{28}Ga_{22}$ alloys with 5 M [15] and in $Ni_{50}Mn_{30}Ga_{20}$ alloys with 7 M [23] modulated structures.

Many recent studies on quasi-ternary Ni–Mn–Ga–X alloys have been directed at the selective partial substitution of 3d elements, Co and Fe [6,24–28]. Substitution of Co for Ni causes an increase

* Corresponding author. Tel.: +91 40 23010241.
E-mail address: seshubai@gmail.com (V. Seshubai).

0925-8388/$ – see front matter © 2011 Elsevier B.V. All rights reserved.
doi:10.1016/j.jallcom.2011.05.064

Table 1
Chemical composition from EDAX, electron per atom ratio, martensitic start (M_s), martensitic finish (M_f), austenite start (A_s) and austenite finish (A_f), martensitic transformation temperature ($T_M = (M_s + M_f + A_s + A_f)/4$) and Curie temperature (T_C) of Co-doped alloys currently studied.

Code	Chemical composition (at.%)	e/a	M_s (K)	M_f (K)	A_s (K)	A_f (K)	T_M (K)	T_C (K)
C-0	$Ni_{49.8}Mn_{29.1}Ga_{21.1}$	7.650	324	305	315	336	320	374
CNi-1.3	$Ni_{49.1}Mn_{28.4}Ga_{21.2}Co_{1.3}$	7.651	309	298	308	316	308	385
CNi-1.9	$Ni_{48.6}Mn_{28.1}Ga_{21.4}Co_{1.9}$	7.640	307	285	295	319	302	393
CNi-2.4	$Ni_{47.7}Mn_{28.8}Ga_{21.1}Co_{2.4}$	7.635	272	264	279	285	275	400
CNi-3.3	$Ni_{46.9}Mn_{28.8}Ga_{21}Co_{3.3}$	7.633	259	250	267	273	262	405
CNi-4.1	$Ni_{46}Mn_{28.5}Ga_{21.4}Co_{4.1}$	7.606	235	230	242	246	238	413
CMn-1.8	$Ni_{49.8}Mn_{27.2}Ga_{21.2}Co_{1.8}$	7.682	316	305	312	327	315	380
CMn-2.4	$Ni_{50.1}Mn_{26}Ga_{21.5}Co_{2.4}$	7.691	316	308	318	327	317	382.5
CMn-3.3	$Ni_{50.3}Mn_{25.2}Ga_{21.3}Co_{3.3}$	7.722	370	361	372	384	372	384
CMn-4.0	$Ni_{50.7}Mn_{24.5}Ga_{20.8}Co_{4.0}$	7.769	373	366	376	386	375	389
CMn-4.7	$Ni_{50.7}Mn_{23.3}Ga_{21.3}Co_{4.7}$	7.763	364	355	370	384	371	391
CMn-6.8	$Ni_{50}Mn_{21.8}Ga_{21.4}Co_{6.8}$	7.780	404	389	423	440	414	398

in the Curie temperature (T_C) and a decrease in the martensitic transformation temperature (T_M) [6,29]. On the other hand, Co replacing Mn has a weak effect on T_C, and causes a large increase of T_M. The variation in T_M follows a general trend that T_M rises with an increase in the average electron per atom (e/a) ratio [6]. The crystal structures of the Ni-excess compositions in the series $Ni_{53-x}Mn_{25}Ga_{22}Co_x$ with $x = 0$ to 14 [29], $Ni_{56-x}Mn_{25}Ga_{19}Co_x$ ($x = 0$, 2–14), $Ni_{56}Mn_{25-y}Ga_{19}Co_y$ ($y = 4$, 8) and $Ni_{56-z/2}Mn_{25-z/2}Ga_{19}Co_z$ ($z = 4$, 6) [30] were all of non-modulated tetragonal symmetry. In the first series from the above, the martensitic transformation was suppressed for compositions with $x > 8$.

The work described above is on Ni-excess compositions, all of which were in the NM tetragonal structure, before and after Co-doping. The alloys $(Ni_{50.26}Mn_{27.30}Ga_{22.44})_{100-x}Co_x$ ($x = 0, 2, 4$ and 6), which do not have excess Ni, were also of non-modulated tetragonal symmetry on Co doping [31]. Since modulated crystal structure is one of the essential criteria for achieving high magnetic strain in FSMA at relatively low magnetic fields, we have chosen to investigate the effect of Co doping in $Ni_{50}Mn_{29}Ga_{21}$ alloy which has 7 M orthorhombic structure in the martensitic state, and displays wide spread twin deformation. This composition is known to exhibit large magnetic field induced strain in single crystals [1], which arises from the high magneto-crystalline anisotropy and low twinning stresses, caused by the modulated crystal structure in the martensitic phase [1,13,23]. This paper aims at a detailed study on the effect of selective partial substitution of Co for Ni, and for Mn, in the compound $Ni_{50}Mn_{29}Ga_{21}$. The aim of the study was to know whether the superstructural ordering could be retained on Co-doping, and as to how the resultant microstructures would be correlated to the changes in crystal structures.

2. Experimental procedures

We have synthesized two different series of polycrystalline alloys with nominal compositions $Ni_{50-x}Mn_{29}Ga_{21}Co_x$ ($x = 0$, 1.5, 2.0, 2.5, 3.5 and 4) and $Ni_{50}Mn_{29-x}Ga_{21}Co_x$ ($x = 0$, 1.5, 2.5, 3.5, 4.0, 4.5 and 6.5) in the present work. These

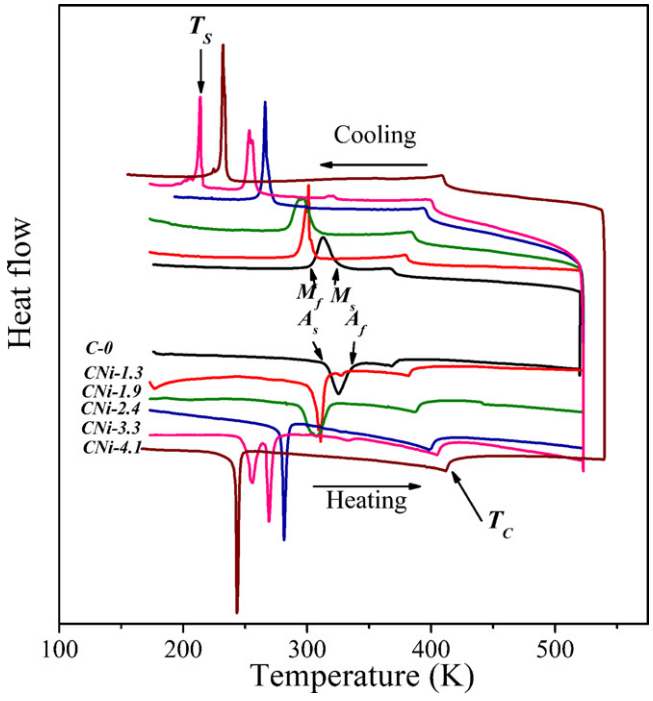

Fig. 1. DSC scans recorded while heating and cooling the alloys of the CNi-x ($x = 0$, 1.3, 1.9, 2.4, 3.3 and 4.1) series. The characteristic temperatures associated with the martensitic transformation, viz. martensitic start (M_s), martensitic finish (M_f), austenite start (A_s) and austenite finish (A_f), and the Curie temperature (T_C) are indicated in the figure. An additional transformation is observed at T_S in the sample CNi-3.3 which is attributed to a change in the local magnetic order and is discussed elsewhere.

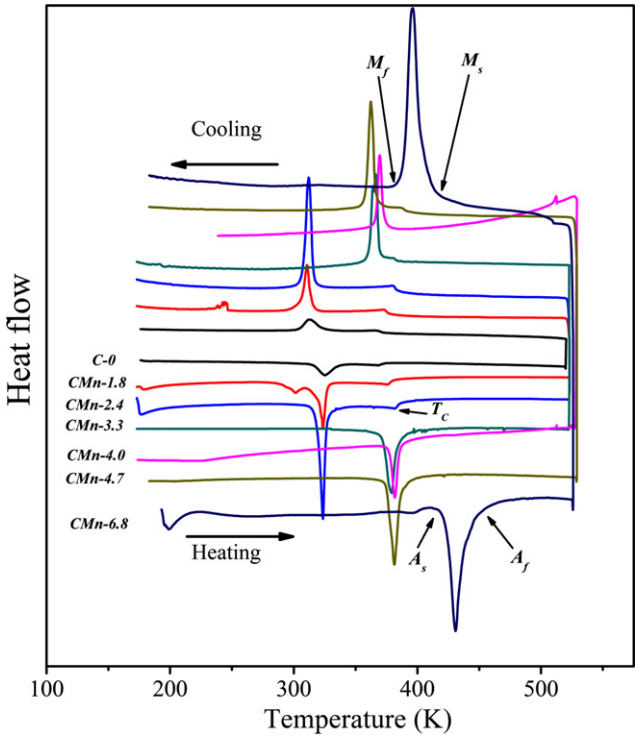

Fig. 2. DSC scans recorded while heating and cooling the alloys of CMn-x ($x = 0$, 1.8, 2.4, 3.3, 4.0, 4.7 and 6.8) series. The characteristic temperatures associated with the martensitic transformation (as discussed in Fig. 1), and the Curie temperatures are indicated in the figure.

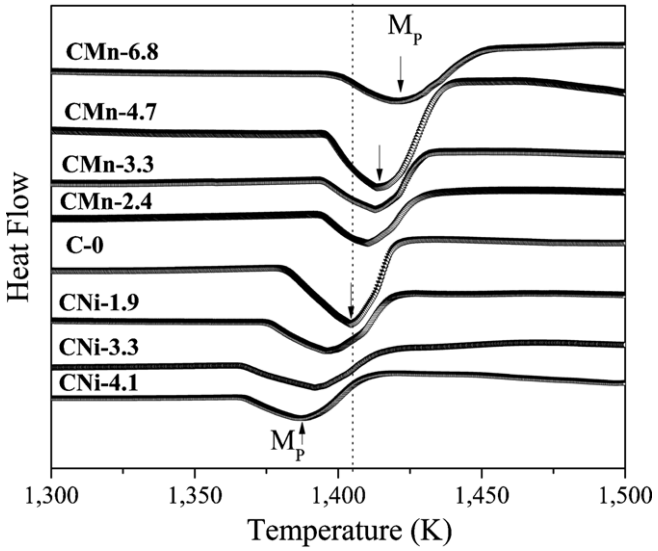

Fig. 3. Differential Thermal Analysis (DTA) scans of the $Ni_{50-x}Mn_{29}Ga_{21}Co_x$ ($x = 0$, 1.9, 3.3 and 4.1) and $Ni_{50}Mn_{29-x}Co_xGa_{21}$ ($x = 0$, 1.8, 2.4, 3.3, 4.7 and 6.8) alloys during heating showing a systematic variation in the melting point of the alloys with Co content.

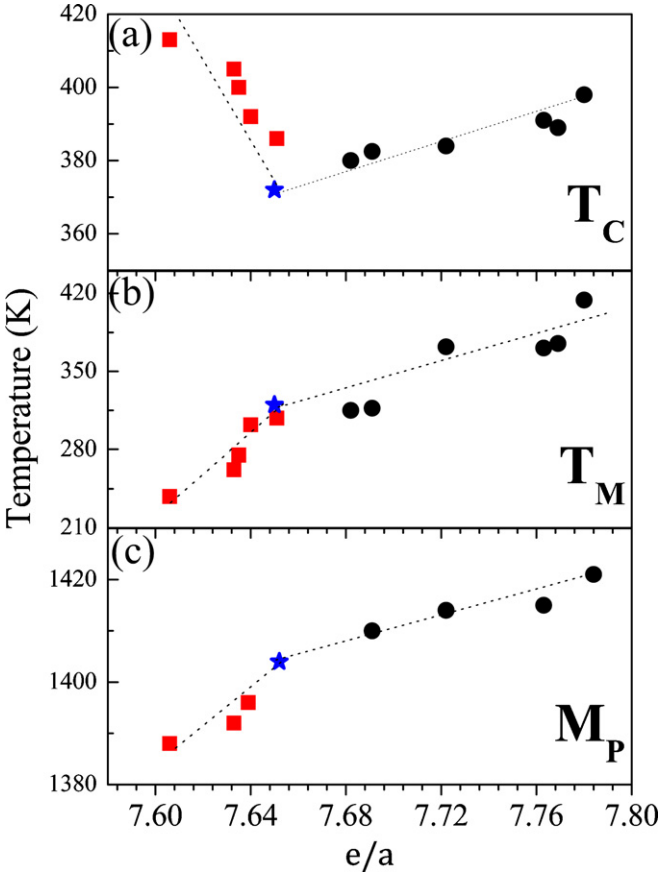

Fig. 4. Variation of (a) Curie temperature (T_C), (b) martensitic transformation temperature (T_M), and (c) melting points, with electron per atom ratio for the parent alloy and the alloys of CNi-x and CMn-x series are shown. The filled squares (red online) stand for the CNi-x series, the filled circles (black online) stand for the CMn-x series, and the star symbol (blue online) stands for the Co-free parent alloy. (For interpretation of the references to color in this figure legend, the reader is referred to the web version of the article.)

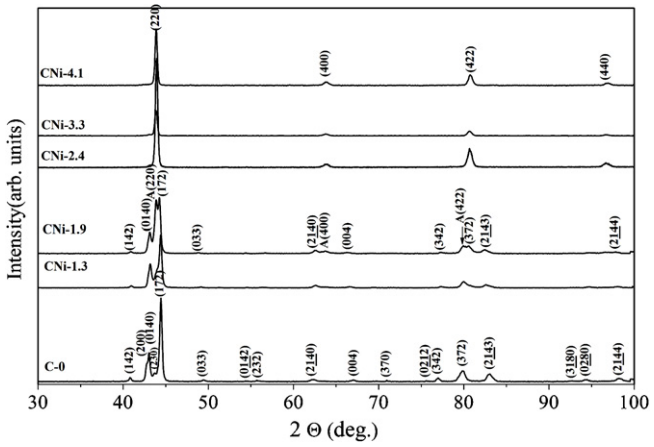

Fig. 5. Powder X-ray diffraction (XRD) patterns from CNi-x ($x = 0$, 1.3, 1.9, 2.4, 3.3 and 4.1) alloys, recorded at RT. In the case of CNi-1.9 alloy, the reflections from austenitic phase are marked with a prefix 'A'.

alloys were prepared by induction melting of appropriate quantities of the constituent elements Ni, Ga and Co of 99.999% purity and Mn of 99.99% purity under argon atmosphere. Loss of Mn up to 2 wt.% by evaporation during melting has been reported [9] in the literature. In our experiments, we had assessed the loss of Mn to be 1.2 wt.% by comparing the starting compositions with the final compositions determined by Energy Dispersive X-ray Analyses (EDAX). Hence 1.2 wt.% of excess Mn was added to adjust for the loss of Mn during melting. The ingots were homogenized under vacuum in quartz ampoules for 8 days at 830 °C and quenched into ice water, following procedures described in the literature [32]. The chemical compositions of the samples were determined using the EDAX facility on a JEOL scanning electron microscope. The martensitic transformation temperatures as well as the Curie temperatures were determined from Differential Scanning Calorimetry (DSC), using a Mettler Toledo DSC1 equipment operated in the temperature range 150–873 K. Melting points of the alloys were determined using a Mettler Toledo DTA1 facility. Fine powders for X-ray diffraction (XRD) studies were prepared by crushing the ingots. They were annealed in argon atmosphere for 12 h at 500 °C followed by furnace cooling, to remove the residual stresses. X-ray diffractograms at ambient temperature were recorded using a Philips X'pert X-ray diffractometer with Cu Kα radiation. The data was collected in the 2θ range of 30–100° using step scan with a step size $\Delta(2\theta) = 0.02°$ and a scan rate of 10 s per step. A circular piece, 3 mm in diameter, was cut from the bulk sample and thinned to electron transparency using a Gatan precision ion polishing system. It was studied using an FEI TECHNAI G^2 transmission electron microscope (TEM) operating at 200 kV. The selected area electron diffraction results were combined with those from XRD to deduce the crystal structure of the materials. The lattice parameters were obtained from the XRD patterns using Philips X'pert plus software.

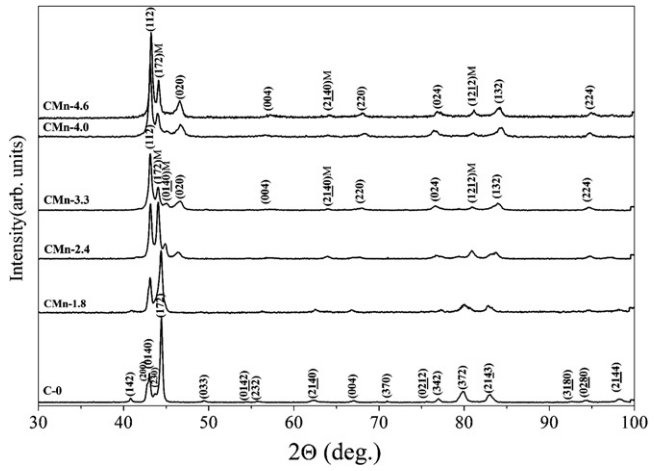

Fig. 6. Powder X-ray diffraction (XRD) patterns from CMn-x ($x = 0$, 1.8, 2.4, 3.3, 4.0 and 4.7) alloys at RT. The additional reflections from modulated orthorhombic crystal structure are marked with a suffix 'M'.

Table 2
The crystal structure at room temperature, lattice parameters: of modulated martensite, non-modulated martensite and cubic structure of Co-doped Ni–Mn–Ga alloys. 7M-O, NM-T and C stand for seven-layer modulated orthorhombic, non-modulated tetragonal and cubic crystal structure respectively.

Code	Crystal structure at RT	Lattice parameters of						
		Modulated martensitic phase			Non-modulated martensitic phase			Austenite phase
		a (Å)	*b* (Å)	*c* (Å)	*a* (Å)	*b* (Å)	*c* (Å)	*a* (Å)
C-0	7M-O	4.208(2)	29.371(1)	5.588(9)	...	...	...	...
CNi-1.3	7M-O	4.192(2)	29.386(7)	5.624(6)	...	...	...	...
CNi-1.9	7M-O + C	4.190(1)	29.429(8)	5.642(2)	...	...	...	5.835(1)
CNi-2.4	C	...	...	...	...	...	...	5.834(4)
CNi-3.3	C	...	...	...	...	...	...	5.835(3)
CNi-4.1	C	...	...	...	...	...	...	5.836(6)
CMn-1.8	7M-O	4.195(1)	29.258(6)	5.598(2)	...	...	...	...
CMn-2.4	7M-O + NM-T	4.190(1)	29.429(8)	5.642(1)	3.905(4)	3.905(4)	6.448(2)	...
CMn-3.3	7M-O + NM-T	4.131(9)	28.832(1)	5.793(2)	3.903(7)	3.903(7)	6.445(9)	...
CMn-4.0	7M-O + NM-T	4.134(2)	28.816(9)	5.791(4)	3.899(2)	3.899(2)	6.428(5)	...
CMn-4.7	7M-O + NM-T	4.137(2)	28.716(3)	5.793(2)	3.897(5)	3.897(5)	6.416(9)	...
CMn-6.8	NM-T	...	...	...	3.876(1)	3.876(1)	6.402(7)	...

3. Results and discussion

The EDAX compositions of the two series of alloys under study, with Co substituted for Ni and for Mn in Ni–Mn–Ga, are given in Table 1. Hereafter the $Ni_{50-x}Co_xMn_{29}Ga_{21}$ alloys with $x = 0.0$, 1.3, 1.9, 2.4, 3.3 and 4.1 will be referred to as C-0, CNi-1.3, CNi-1.9, CNi-2.4, CNi-3.3, and CNi-4.1 respectively. Similarly, the $Ni_{50}Mn_{29-x}Co_xGa_{21}$ alloys $x = 0.0, 1.8, 2.4, 3.3, 4.0, 4.7$ and 6.8 will be referred to as C-0, CMn-1.8, CMn-2.4, CMn-3.3, CMn-4.0, CMn-4.7 and CMn-6.8 respectively.

3.1. Martensitic transformations

DSC scans recorded during heating and cooling cycles, for the alloys of the CNi-*x* and CMn-*x* series respectively, are shown in Figs. 1 and 2. The characteristic transformation temperatures i.e., martensitic start (M_s), martensitic finish (M_f), austenite start (A_s) and austenite finish (A_f) are determined for the alloys and presented in Table 1. Fig. 3 shows DTA scans of CNi-*x* ($x = 0$, 1.9, 3.3 and 4.1) and CMn-*x* ($x = 2.4$, 3.3, 4.7, 6.8) series during heating; the melting points of the alloys are indicated in the figure. Fig. 4(a) and (b) shows the variation of the martensitic transformation temperatures $T_M = (M_s + M_f + A_s + A_f)/4$, the Curie temperatures T_C, and the melting points (M_P) of the alloys as function of the electron per atom ratio (e/a). The e/a values were computed taking the elemental valences for Ni, Co, Mn and Ga to be 10, 9, 7 and 3 respectively, as done in literature [33]. It is observed that T_C increases with cobalt content in both the series, but the variation is much faster when cobalt is substituted for nickel than for Mn. T_M gradually decreases on substitution of Co for Ni while it increases non-linearly on substitution of Co for Mn. The melting points exhibit a variation similar to that of martensitic transformation temperatures with e/a, as can be seen from Fig. 4. This study shows that in addition to T_M and T_C, the melting points also depend on whether Co is substituted for Ni or Mn. In the CNi-3.3 alloy, an additional first order transformation is observed (at T_s), just below the martensitic transformation temperature. Detailed magnetization measurements on the sample showed that this transformation is possibly associated with partial inversion of magnetic moments locally and the details will be reported elsewhere [34]. The other small thermal effects seen in the DSC scan around 330 K can be associated with pre-martensitic transformations [5].

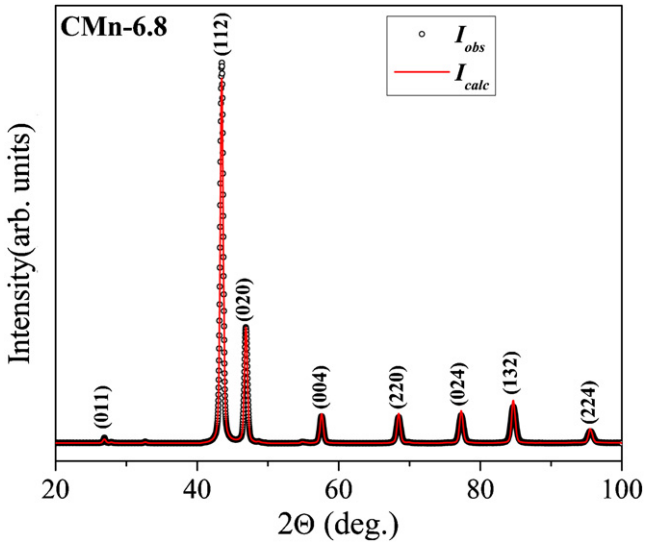

Fig. 7. Powder X-ray diffraction pattern from the CMn-6.8 alloy at RT. The circles indicate the experimental data while the line represents the profile obtained from a Rietveld analysis.

3.2. Crystal structure

3.2.1. $Ni_{50-x}Mn_{29}Ga_{21}Co_x$ ($x = 0$, 1.3, 1.9, 2.4, 3.3 and 4.1) alloys

Fig. 5 shows the XRD patterns of the CNi-*x* series of alloys recorded at room temperature (RT). The pattern of C-0 is indexed to an orthorhombic unit cell with 7-layer modulation (7 M) in the b-direction. The lattice parameters computed using the XRD pattern are given in Table 2. These values agree well with those reported in literature [10] for this composition. Alloy CNi-1.3 also exhibits 7 M orthorhombic structure similar to that of the parent alloy. In samples with higher concentrations of cobalt substituted for nickel, the crystal structure transforms gradually from 7 M orthorhombic to cubic $L2_1$ structure at RT. In CNi-1.9 alloy, we find that the austenitic and martensitic phases coexist at RT; this is because its T_M (302 K) is very close to RT. The XRD pattern from the CNi-1.9 alloy is indexed to a combination of martensitic and austenitic phases, and the weight fraction of the austenitic phase is found to be 60% at RT using the Rietveld analysis. The CNi-2.4, CNi-3.3 and CNi-4.1 alloys are 100% austenitic at RT, and their T_M are below RT. The patterns are indexed to cubic $L2_1$ structure. The lattice parameters for the cubic phase are also given in Table 2.

3.2.2. $Ni_{50}Mn_{29-x}Co_xGa_{21}$ ($x = 0$, 1.8, 2.4, 3.3, 4.0, 4.7 and 6.8) alloys

The XRD patterns recorded at RT in the CMn-*x* series of alloys, with cobalt-doped for manganese, are shown in Fig. 6. All the

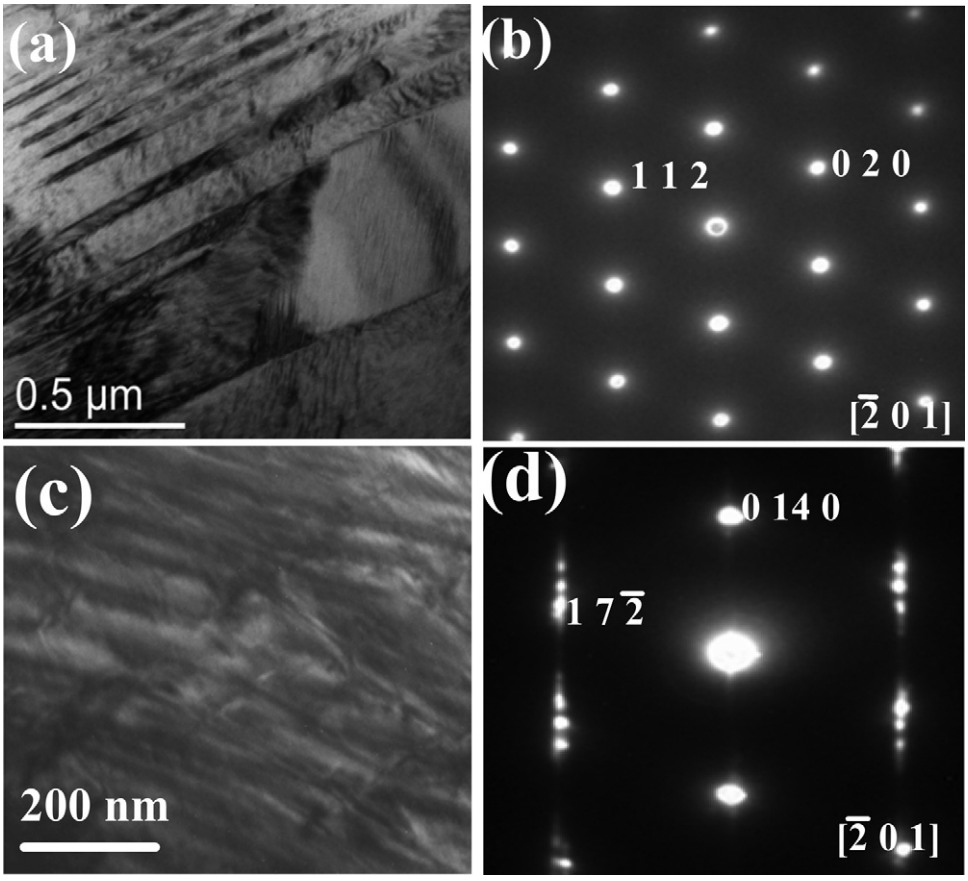

Fig. 8. (a) TEM bright field image from a region in the CMn-3.3 alloy and (b) the corresponding SAED pattern, indexed to non-modulated tetragonal crystal structure, (c) bright field image of another region in the same alloy and (d) the corresponding SAED pattern indexed to 7 M orthorhombic structure. These observations confirm that some amount of 7 M orthorhombic phase co-exists with the majority non-modulated tetragonal phase.

alloys of this series are in martensitic state at RT. The CMn-1.8 alloy crystallizes in 7 M orthorhombic structure similar to C-0. In Fig. 7, the pattern obtained from the CMn-6.8 alloy at RT is shown which is indexed to non-modulated tetragonal structure (NM), with *I*4/*mmm* space group. The calculated pattern using Rietveld refinement technique is shown along with the observed pattern, and a good agreement can be observed between the observed and calculated profiles. The lattice parameters of the CMn-6.8 alloy is determined to be $a = 3.876(1)$ Å and $c = 6.402(7)$ Å with axial ratio c/a of 1.65. These lattice parameters are comparable to those reported in literature [35] for $Ni_{58.0}Mn_{19.4}Ga_{22.6}$ alloy that crystallizes in non-modulated tetragonal structure.

The pattern for CMn-3.3 has similarity to that of CMn-6.8 except for the extra reflections at angles (2θ) of 44.1°, 45°, 64° and 81.3°. To get more insight into the origin of the additional reflections, TEM investigations have been carried out in CMn-3.3 alloy. In Fig. 8, we show TEM bright field images and Selected Area Electron Diffraction (SAED) patterns recorded in two different regions of CMn-3.3 alloy. Fig. 8(a) shows a TEM bright field image from one of the regions displaying martensitic twin variants of widths in a few nanometers. Fig. 8(b) shows a SAED pattern from the same region. This [$\bar{2}$ 0 1] zone axis pattern is indexed to a tetragonal unit cell ($a = b = 3.91$ Å, $c = 6.46$ Å). No spots corresponding to a superstructure cell were observed in this region. A search in different regions of the sample showed the presence of small amounts of a phase with 7 M orthorhombic structure, in a few regions. The corresponding bright field image and SAED are shown in Fig. 8(c) and (d) respectively. Based on TEM observations on the CMn-3.3 alloy, the XRD reflections of the alloy shown in Fig. 6 have been indexed to an admixture of non-modulated tetragonal phase and a 7 M orthorhombic phase. By Rietveld analysis, the ratio of the NM tetragonal phase to the 7 M orthorhombic phase was calculated to be 80:20. The estimated lattice parameters from the two phases in CMn-3.3 alloy are given in Table 2. XRD patterns of CMn-2.4, CMn-4.0 and CMn-4.7 were also identified as admixtures of

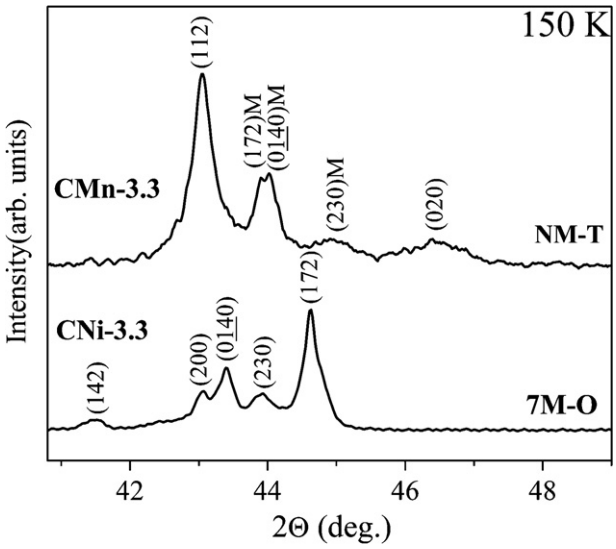

Fig. 9. XRD patterns recorded at 150 K in CNi-3.3 and CMn-3.3 alloys. The pattern from CNi-3.3 is indexed to a 7 M orthorhombic unit cell and that from CMn-3.3 to a mixture of NM and 7 M unit cells. Suffix 'M' stands for reflections from the 7 M phase in the pattern of the CMn-3.3 alloy.

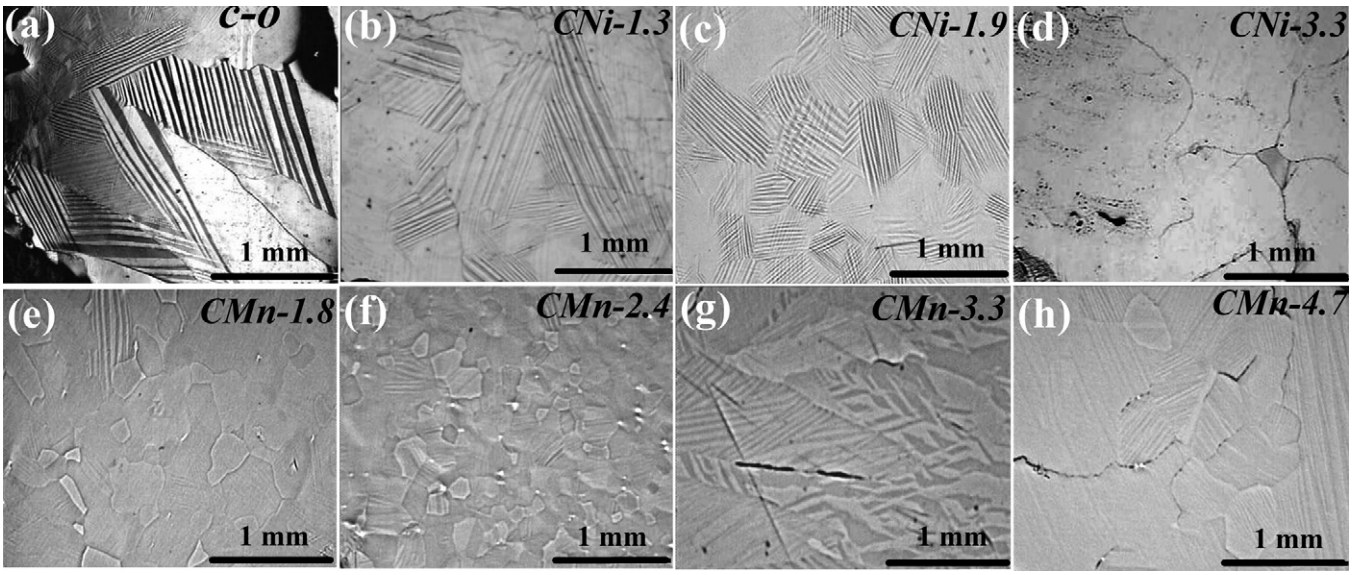

Fig. 10. The figure shows optical micrographs from C-0, CNi-*x* and CMn-*x* alloys at RT. (a) and (b) show widespread twining in the alloy with 7 M crystal structure. In (c), short-range twin variants along with regions without twinning are seen in CNi-1.9 alloy which is a mixture the 7 M and cubic austenitic phases. In (d), the austenite phase shows no twinning. (e)–(h) Show sporadic appearance of small islands within which twin variants occur on a fine scale for the alloys of the CMn-*x* series.

the two phases. The percentage of the non-modulated martensitic phase increases with cobalt substitution for Mn: and it amounts to nearly 40% at $x = 2.4$, to 80% at $x = 3.3$, and 90% at $x = 4.7$. At $x = 6.8$, the alloy is a fully non-modulated martensite with tetragonal structure. Compositions with higher Co content were explored in the case of the CMn-*x* series of alloys, unlike in the case of the CNi-*x* series, so as to confirm the occurrence of the NM tetragonal phase in single-phase form.

XRD measurements were performed at 150 K to investigate the structures of CNi-3.3 and CMn-3.3 alloys at low temperatures where both the alloys are in martensitic phase (see Fig. 9). The CNi-3.3 alloy which is a cubic austenite at RT is observed to transform to be a martensite with 7 M orthorhombic crystal structure at lower temperatures ($a = 4.18$ Å, $b = 29.46$ Å and $c = 5.65$ Å). The majority phase in CMn-3.3 alloy which is in martensitic state at RT, retains its non-modulated tetragonal structure to low temperatures, except that it shows a small variation in the lattice parameters.

We see from the above that the behavior of the substituted alloys is very different depending on whether cobalt is substituted for Ni, or for Mn, in $Ni_{50}Mn_{29}Ga_{21}$. In the case of Co substitution for Ni, the alloy retains the 7 M orthorhombic structure in the martensitic state just as the parent phase. On the other hand, substitution of Co for Mn in concentrations above 1.8% causes the stabilization of non-modulated tetragonal structure in the martensitic state. These observations show that the selective substitution of cobalt for Ni or Mn has a significant role in deciding the structural ordering in

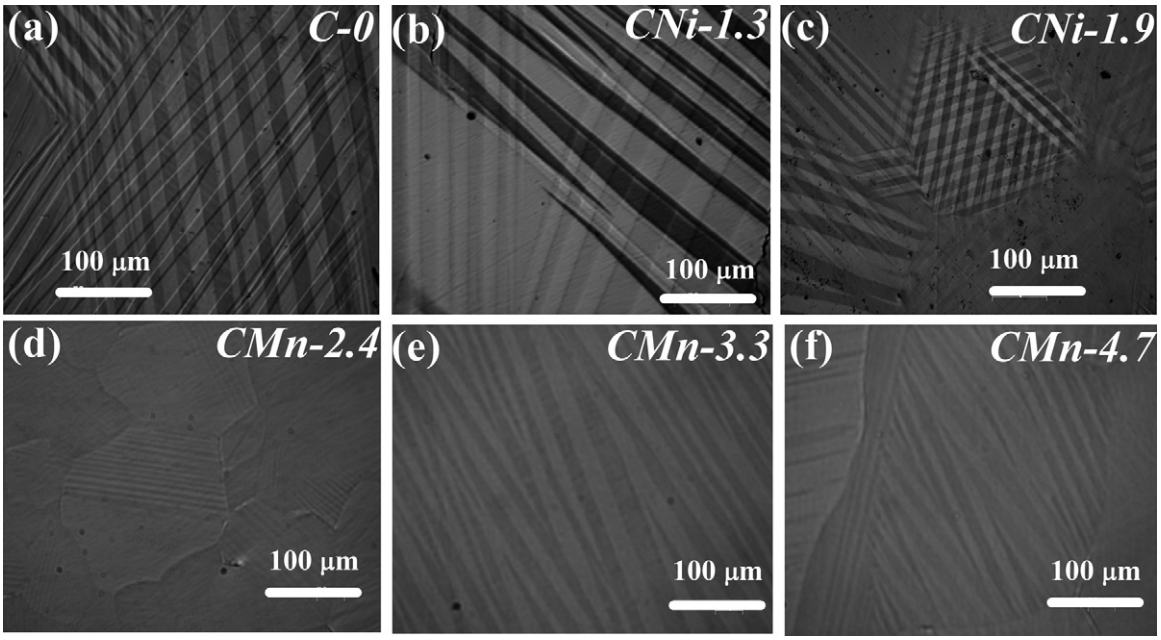

Fig. 11. The figure shows microstructures recorded at magnification higher than that in Fig. 10. (a)–(c) Show that alloys with Co-doped for Ni, which have 7 M orthorhombic structure, exhibit widespread crossing twins. (d)–(f) Show that alloys with Co-doped for Mn, which have non-modulated tetragonal phase, show faint parallel twin variants within islands and do not exhibit any crossing twins.

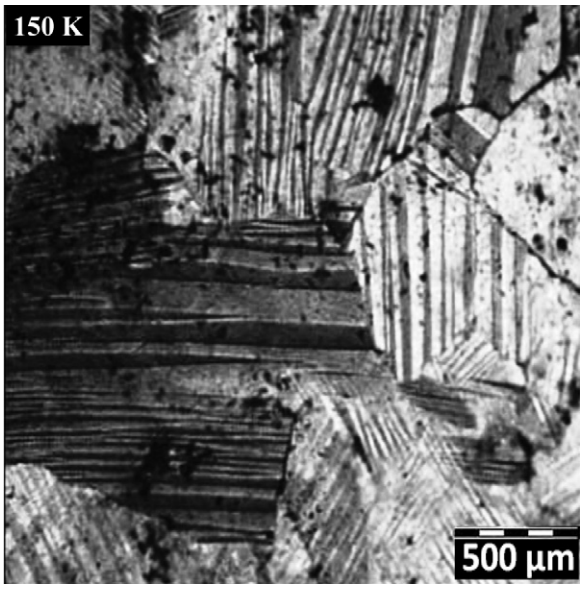

Fig. 12. Widespread twin variants characteristic of 7 M orthorhombic structure is observed when the CNi-3.3 alloy is cooled to 150 K. The alloy which is cubic at RT, has a martensitic 7 M structure at 150 K as seen from Fig. 9.

addition to influencing the T_M and T_C. An examination of the atomic volumes [36–38] of the elements involved reveals that substitution of Co, whose atomic volume (V_{Co}) is 6.7 cm^3/mol, for Ni (with V_{Ni} = 6.6 cm^3/mol) causes an atomic volume change of only 1.7%. On the other hand, substitution of Co for Mn (V_{Mn} = 7.4 cm^3/mol) causes 9.5% volume change. This possibly induces a large localized stress when Co is doped for Mn and suppresses the superstructural ordering, while substitution of Co for Ni does not seem to affect it. The effect of atomic volume change is also reflected in the microstructures, as will be discussed in the next section.

3.3. Microstructure

Fig. 10 shows the optical microstructures recorded in polycrystalline specimens in the martensitic phase, after polishing down to 0.25 μm. Fig. 10(a) shows the martensitic twin variants of the Co-free composition C-0, with parallel bands-like morphology and crossing of thermo-elastic martensite variants. These are spread over the entire sample indicating long-range deformation. The microstructure of CNi-1.3 shown in Fig. 10(b) is similar to that of C-0. Fig. 10(c) shows that well-defined twins are absent in a few regions in CNi-1.9 at RT, which is close to T_M, supporting the picture of coexisting austenitic and martensitic phases as deduced from XRD pattern. The microstructures of the alloys CNi-3.3 (Fig. 10(d)) and CNi-4.1 (not shown) did not show any twin variants since they are in cubic austenite phase at RT. In contrast, the microstructures of all the alloys with Co-doped for Mn, shown in Fig. 10(e)–(h), do exhibit twins but only in the form of sporadic islands. Faint twin variants are found within the islands and long-range deformation is conspicuously absent. Fig. 11 recorded at higher magnification shows that C-0, CNi-1.3 and CNi-1.9 alloys with 7 M orthorhombic structure exhibit widespread crossing twins that is indicative of low residual stresses suitable for large shape memory effect [22], whereas the alloys with Co-doped for Mn do not exhibit any such crossing twins. It can be seen that there is a strong correlation between structural ordering and the nature of twin variants formed in the resultant microstructures in martensitic state. This is also confirmed by the microstructure recorded in CNi-3.3 alloy in the martensitic state by cooling the sample to 150 K, which is shown in Fig. 12. In the figure, widespread twin variants and crossing twins can be seen, which are typical of 7 M orthorhombic structure of the parent alloy. This microstructure is similar to that observed in C-0 and CNi-1.3 at RT (Fig. 10).

4. Conclusions

The effect of cobalt substitution for Ni or Mn in $Ni_{50}Mn_{29}Ga_{21}$ alloy with 7 M orthorhombic structure is investigated. The crystal structure, martensitic and magnetic transformation temperatures (T_M and T_C) and the microstructure of Co-doped alloys are presented. The results reveal that the crystal structure/ordering and microstructure are strongly correlated. Substitution of Co for Ni which causes only 1.7% difference in atomic volume locally does not alter the superstructural ordering and long range twin deformation. In contrast, substitution of Co for Mn involves a volume change of 9.5% locally and, due to possible local stresses, it suppresses superstructural ordering and results in the observation of sporadic islands within which twin variants are confined. Our results demonstrate that the change in crystal structure and the resultant microstructures depend on the concentration of Co, and on whether it is substituted for Ni whose atomic size comparable to that of Co, or for Mn which differs in size considerably from Co.

Acknowledgements

Funding from Aeronautical Development Agency (ADA), Bangalore in the form of a project (ref. no. ADA/AF/DISMAS/163/2005) is gratefully acknowledged. ASK thanks CSIR (Ref. No. 03 (1065) 106/EMR-II) and MR thanks UGC-RFSMS for fellowship. The authors are thankful to Dr. K. Muraleedharan and Mr. Deepak Kumar, DMRL for the sample preparation for TEM studies.

References

[1] A. Sozinov, A.A. Likhachev, K. Ullakko, IEEE Trans. Magn. 38 (2002) 2814–2816.
[2] Y. Xin, Y. Li, Z. Liu, Scripta Mater. 63 (2010) 35–38.
[3] P. Entel, V.D. Buchelnikov, M.E. Gruner, A. Hucht, V.V. Khovailo, S.K. Nayak, A.T. Zayak, Mater. Sci. Forum 583 (2008) 21–41.
[4] A. Planes, L. Manosa, M. Acet, J. Phys.: Condens. Matter 21 (2009) 233201–1233201.
[5] M. Zeng, S. Wing Or, Z. Zhu, S.L. Ho, J. Appl. Phys. 108 (2010) 053716–053720.
[6] D.E. Soto-Parra, X. Moya, L. Mañosa, A. Planes, H. Flores-Zúñiga, F. Alvarado-Hernández, R.A. Ochoa-Gamboa, J.A. Matutes-Aquino, D. Ríos-Jara, Philos. Mag. 90 (2010) 2771–2792.
[7] J. Chen, Y. Li, J. Shang, H. Xu, J. Phys.: Condens. Matter 21 (2009) 045506–045513.
[8] X.Q. Chen, F.J. Yang, X. Lu, Z.X. Qin, Phys. Status Solidi (b) 244 (2007) 1047–1053.
[9] B.R. Gautam, I. Dubenko, A.K. Pathak, S. Stadler, N. Ali, J. Magn. Magn. Mater. 321 (2009) 29–33.
[10] R.K. Singh, M. Manivel Raja, R.P. Mathur, M. Shamsuddin, J. Alloys Compd. 506 (2010) 73–76.
[11] S.Y. Yu, Z.X. Cao, L. Ma, G.D. Liu, J.L. Chen, G.H. Wu, B. Zhang, X. Zhang, Appl. Phys. Lett. 91 (2007) 102507–102510.
[12] S. Fabbrici, J. Kamarad, Z. Arnold, F. Casoli, A. Paoluzi, F. Bolzoni, R. Cabassi, M. Solzi, G. Porcari, C. Pernechele, F. Albertini, Acta Mater. 59 (2011) 412–419.
[13] V. Sanchez-Alarcos, J.I. Perez-Landazabal, V. Recarte, G.J. Cuello, Acta Mater. 55 (2007) 3883–3889.
[14] B. Wedel, M. Suzuki, Y. Murakami, C. Wedel, T. Suzuki, D. Shindo, K. Itagaki, J. Alloys Compd. 290 (1999) 137–143.
[15] Z. Li, Y. Zhang, C. Esling, X. Zhao, L. Zuo, Acta Mater. 59 (2011) 3390–3397.
[16] R. Ranjan, S. Banik, S.R. Barman, U. Kumar, P.K. Mukhopadhyay, D. Pandey, Phys. Rev. B 74 (2006) 224443–224450.
[17] L. Righi, F. Albertini, E. Villa, A. Paoluzi, G. Calestani, V. Chernenko, S. Besseghini, C. Ritter, F. Passaretti, Acta Mater. 56 (2008) 4529–4535.
[18] O. Söderberg, D. Brown, I. Aaltio, J. Oksanen, J. Syrén, H. Pulkkinen, S.P. Hannula, J. Alloys Compd. 509 (2011) 5981–5987.
[19] U. Gaitzsch, M. Potschke, S. Roth, N. Mattern, B. Rellinghaus, L. Schultz, J. Alloys Compd. 443 (2007) 99–104.
[20] V.A. Chernenko, M. Chmielus, P. Müllner, Appl. Phys. Lett. 95 (2009) 104103–104106.
[21] O. Söderberg, Laboratory of Physical Metallurgy and Materials Science, Helsinki University of Technology, Doctoral Thesis TKK-ME-DT-2 (2004).
[22] M. Ramudu, A. Satish Kumar, V. Seshubai, K. Muraleedharan, K.S. Prasad, T. Rajasekharan, Scripta Mater. 63 (2010) 1073–1076.
[23] Z.B. Li, Y.D. Zhang, C. Esling, X. Zhao, L. Zuo, Acta Mater. 59 (2011) 2762–2772.

[24] D.E. Soto-Parra, F. Alvarado-Hernandez, O. Ayala, R.A. Ochoa-Gamboa, H. Flores-Zuniga, D. Rios-Jara, J. Alloys Compd. 464 (2008) 288–291.
[25] C. Seguí, E. Cesari, Intermetallics 19 (2011) 721–725.
[26] S. Yan, J. Pu, B. Chi, L. Jian, J. Alloys Compd. 507 (2010) 331–334.
[27] K. Rolfs, M. Chmielus, R.C. Wimpory, A. Mecklenburg, P. Müllner, R. Schneider, Acta Mater. 58 (2010) 2646–2651.
[28] S. Yang, Y. Ma, H. Jiang, X. Liu, Intermetallics 19 (2011) 225–228.
[29] D.Y. Cong, S. Wang, Y.D. Wang, Y. Ren, L. Zuo, C. Esling, Mater. Sci. Eng. A 473 (2008) 213–218.
[30] Y.Q. Ma, S.Y. Yang, Y. Liu, X.J. Liu, Acta Mater. 57 (2009) 3232–3241.
[31] V. Sanchez-Alarcos, J.I. Peĭrez-Landazabal, V. Recarte, C. Gomez-Polo, J.A. Rodrıguez-Velamazan, Acta Mater. 56 (2008) 5370–5376.
[32] A.N. Vasil'ev, A.D. Bozhko, V.V. Khovailo, I.E. Dikshtein, V.G. Shavrov, V.D. Buchelnikov, M. Matsumoto, S. Suzuki, T. Takagi, J. Tani, Phys. Rev. B 59 (1999) 1113–1120.
[33] V.A. Chernenko, Scripta Mater. 40 (1999) 523–527.
[34] A. Satish Kumar, M. Ramudu, V. Seshubai, J. Magn. Magn. Mater. (unpublished).
[35] M. Han, J.C. Bennett, M.A. Gharghouri, J. Chen, C.V. Hyatt, N. Mailman, Mater. Charact. 59 (2008) 764–768.
[36] M.L. Richard, J. Feuchtwanger, S.M. Allen, R.C. O'Handley, P. Lazpita, J.M. Barandiaran, J. Gutierrez, B. Ouladdiaf, C. Mondelli, T. Lograsso, D. Schlagel, Philos. Mag. 23 (2007) 3437–3447.
[37] J.K.A. Gschneidner, Solid State Phys. 16 (1964) 276.
[38] J. Janak, A.R. Willams, Phys. Rev. B 14 (1976) 4199–4204.